C. R. Chimie 21 (2018) 61–70

Contents lists available at ScienceDirect

Comptes Rendus Chimie

www.sciencedirect.com

Full paper/Mémoire

Fabrication of hierarchical ZnSAPO-34 by alkali treatment with improved catalytic performance in the methanol-to-olefin reaction

Chao Sun, Yaquan Wang*, Zhao Wang, Hengbao Chen, Xiao Wang, Hongyao Li, Liying Sun, Chunyang Fan, Cui Wang, Xu Zhang

Key Laboratory for Green Chemical Technology of Ministry of Education, School of Chemical Engineering & Technology, Tianjin University, Tianjin 300072, PR China

ARTICLE INFO

Article history:
Received 27 August 2017
Accepted 21 November 2017
Available online 22 December 2017

Keywords:
ZnSAPO-34
Hierarchical zeolite
Alkali treatment
Tetraethylammonium hydroxide
Methanol to olefin

ABSTRACT

A series of hierarchical ZnSAPO-34 zeolites were synthesized by treatment with different concentrations of tetraethylammonium hydroxide (TEAOH) solutions. The synthesized samples were characterized by X-ray diffraction, scanning electron microscopy (SEM), transmission electron microscopy (TEM), inductively coupled plasma optical emission spectroscopy (ICP-OES), temperature-programmed desorption, Fourier transform infrared, and N_2 adsorption and desorption techniques and studied as catalysts for the methanol to olefin reaction. The characterization results reveal that the crystal size of ZnSAPO-34 is greatly reduced compared with the parent SAPO-34 owing to the incorporation of Zn. Hierarchical pores with the sizes up to the macropore level in the ZnSAPO-34 zeolites are created with the post-treatment of TEAOH. The acid strength and the amounts of the strong acid of the hierarchical ZnSAPO-34 zeolites decrease after the post-treatment because TEAOH preferentially extracts Si species from the zeolite. The hierarchical ZnSAPO-34 zeolites exhibit superior catalytic performance than that of the parent ZnSAPO-34, owing to the shortened transportation distance and the appropriate acidity of the treated samples.

1. Introduction

Light olefins, such as ethylene and propylene, are important raw materials in the petrochemical industry, which are mainly produced from naphtha thermal cracking in the past decades. In recent years, immense efforts have been put into developing alternative non-petroleum routes and effective catalytic processes for the production of the light olefins due to the inevitable exhaustion of crude oil in the foreseeable future. Because the inexpensive methanol could be easily produced from coal or natural gas, methanol to olefin (MTO) process based on acidic zeolite catalysts has become one of the most promising alternative routes [1,2].

The electrically neutral aluminophosphate (AlPO) zeolites have no catalytic capabilities owing to the lack of active sites. Accordingly, the isomorphous substitution of silicon atoms into the AlPO framework is the key point for forming silicoaluminophosphate (SAPO) with negatively charged lattice and generating acid sites [3]. Among the SAPOs, SAPO-34 with chabazite structure has been proved to exhibit extraordinary catalytic performance for producing a maximum selectivity of light olefins in the MTO process [4–8]. The large cavities connected by eight rings, relatively mild acidity and high thermal/hydrothermal stability are the favorable

* Corresponding author.
E-mail address: yqwang@tju.edu.cn (Y. Wang).

https://doi.org/10.1016/j.crci.2017.11.006
1631-0748/

characteristics of SAPO-34 for catalyzing the MTO reaction [7–11]. However, similar to other types of zeolites, this superior selectivity of SAPO-34 is often coupled with diffusion limitation and serious pore blocking, owing to the small sizes of its apertures and cavity channels. As a consequence, SAPO-34 deactivates fast, also with a remarkable decrease in selectivity [12–14]. Generally, nanosized zeolites or hierarchical zeolites could mitigate this intrinsic problem through facilitating the access and the transportation of molecules [15–19]. Various synthetic routes have been tried to fabricate nanosized SAPO-34 crystals, which all use the tetraethylammonium hydroxide (TEAOH) in these processes [20–22]. Consequently, intensive studies have been focused on integrating mesopores or/and macropores into microporous structures for the preparation of hierarchical zeolites, including bottom-up and top-down approaches. The traditional bottom-up approach can be categorized into hard- and soft-templating routes with the use of sacrificial mesoporogens during the zeolite synthesis [23–27]. After the combustion of these sacrificial species at elevated temperature, pores are left behind in the zeolite matrix. Unfortunately, the low crystallinity of the resulting product can be an obstacle [28]. Alternatively, the typical top-down method, also known as demetallization method, involves postsynthesis modification of zeolites in an acidic or basic solution [29]. Recently, efforts have been attempted to accelerate the transportation rate by the demetalation approach to introduce secondary larger (meso or macro) pores into the framework of SAPO-34, which could improve the catalytic performance compared with their microporous counterpart. Liu et al. [30] reported that hierarchical SAPO-34 crystals prepared by the TEAOH etching post-treatment displayed a prolonged lifetime in the MTO reaction. Chen et al. [12] prepared hierarchical SAPO-34 crystals in fluoride medium, which exhibited improved catalytic performances in the MTO reaction. Chen et al. [31] also reported that hierarchically structured SAPO-34 crystals formed by the fluoride post-treated route under ultrasonic condition showed an enhanced selectivity of light olefins in the MTO reaction. Qiao et al. [32] created hollow SAPO-34 single crystals via alkaline or acid etching, which showed improved catalytic performance in the alkylation reaction of benzene with benzene alcohol.

It is well established that the incorporation of transition metals into the SAPO framework usually creates additional modifications on the pristine materials [33]. Accordingly, to improve the light olefin selectivity and/or long catalytic lifetime, many metals (Me) have been introduced into the SAPO-34 framework by isomorphous substitution for the formation of-MeSAPO-34 zeolites [34]. For example, Zn-containing SAPO-34 (ZnSAPO-34) zeolites were synthesized with improved $C_2^=-C_3^=$ selectivity in MTO reactions [35]. However, the serious coke formation is still an inevitable problem for -MeSAPO-34.

To the best of our knowledge, the catalytic performance of hierarchical -MeSAPO-34 zeolites in the MTO reaction has not been investigated. Therefore, to fully explore the potential of ZnSAPO-34, we developed a facile way to improve the catalytic performance of ZnSAPO-34 in the MTO process by the construction of hierarchical ZnSAPO-34 with the post-treatment of TEAOH. The hierarchical ZnSAPO-34 zeolites exhibit a significantly improved $C_2^=-C_3^=$ selectivity and a longer catalytic lifetime in the MTO reaction.

2. Experimental section

2.1. Materials

Pseudoboehmite (68% Al_2O_3) was obtained from CHALCO Shandong Co., Ltd., China. $Zn(NO_3)\cdot 6H_2O$ (analytical reagent), quartz sand (20–40 mesh), and phosphoric acid (85 wt %) were purchased from Tianjin Guangfu Fine Chemical Research Institute Co., Ltd., China. Methanol (analytical reagent) and triethylamine (TEA, 99 wt % aq soln) were purchased from Tianjin Jiangtian Fine Chemical Research Institute Co., Ltd., China. Silica sol (40 wt % suspension in water) was purchased from Qingdao Haiyang Chemical Co., Ltd., China. TEAOH (35 wt % aq soln) was obtained from Zhenjiang Runjing High Purity Chemical Co., Ltd., China.

2.2. Synthesis of parent ZnSAPO-34

ZnSAPO-34 was synthesized using TEA as the organic template with a hydrothermal method. The molar composition of the synthesis solution was 1 Al_2O_3:0.6 SiO_2:1 P_2O_5:50 H_2O:3 TEA:0.04 $Zn(NO_3)_2\cdot 6H_2O$. In detail, the gels were prepared by first mixing 3.82 g of pseudoboehmite with 19.26 g of deionized water and then 5.87 g of phosphoric acid was added dropwise. After vigorously stirring for 1 h, 2.29 g of silica sol was added into the resultant solution slowly, followed by continuous stirring for another 5 min. Subsequently, 0.30 g $Zn(NO_3)_2\cdot 6H_2O$ was introduced into the mixture, which was then stirred for an additional 1 h before 7.81 g TEA was added. The reaction gels were further stirred at ambient temperature for 2 h until homogeneous gels were obtained. The gels were sealed in a Teflon-lined autoclave and aged at 120 °C for 24 h, and then crystallized at 200 °C for 48 h under the autogenous pressure. The solid product was separated by repeated cycles of centrifuging and washing until the pH = 7. The product was dried at 120 °C overnight, followed by calcination in air at 550 °C for 5 h to remove the template.

The conventional microporous SAPO-34 sample was synthesized by following the procedure of the ZnSAPO-34 synthesis mentioned above, except that no $Zn(NO_3)_2\cdot 6H_2O$ was added to the gel.

2.3. Preparation of hierarchical ZnSAPO-34

Alkali treatment of the parent ZnSAPO-34 zeolite was performed with 0.1, 0.3, 0.5, and 0.7 mol L^{-1} aqueous TEAOH solutions (15 mL g^{-1} of zeolite) for 1 h at ambient temperature. Then, the solid product was immediately separated by centrifugation and thoroughly washed using distilled water until a neutral pH value was achieved. The resulting samples were dried overnight at 120 °C and calcined in air at 550 °C for 6 h. The alkaline-treated samples were designated as ZnSAPO-34-*x*, in which *x* refers to the concentration of the TEAOH solution.

2.4. Characterization

X-ray diffraction (XRD) patterns were obtained at room temperature on a Rigaku D/max2500 diffractometer using the graphite filtered Cu Kα radiation ($\lambda = 0.1542$ nm) with a scanning rate of 8° min^{-1} in the 2θ ranges from 5° to 50°. The relative crystallinity of the catalysts was calculated by comparing the sum of the peak intensities at $2\theta = 9.4°–9.6°$, 13.0°–13.1°, 20.8°–21.0°, and 31°–31.2° with that of the parent ZnSAPO-34 being defined as 100%.

Scanning electron microscopy (SEMs) were recorded using an S-4800 field-emission scanning electron microscope of Hitachi with an accelerating voltage of 3 kV.

Fourier transform infrared (FTIR) spectra of the catalysts were recorded using a Bruker Vertex 7.0 FTIR spectrometer with a KBr wafer technique. The infrared absorbance spectrum was recorded from 4000 to 400 cm^{-1} at 4 cm^{-1} optical resolution.

Nitrogen adsorption and desorption isotherms were obtained using a Micromeritics ASAP 2020 system. The specific surface areas (S_{BET}) were calculated by the Brunauer–Emmett–Teller (BET) equation. The micropore surface areas and micropore volumes were derived from the *t*-plot method. The total pore volume (V_{total}) was evaluated at $p/p_0 = 0.99$. External surface area (S_{ext}) was calculated by subtracting S_{micro} from S_{BET}. Secondary macropore volume (V_{sec}) was calculated by subtracting V_{micro} from V_{total}.

Temperature-programmed desorption of ammonia (NH_3-TPD) profiles were obtained using a Xianquan TP-5076 TPD analyzer with a thermal conductivity detector.

The coke amounts after reaction were determined using Shimadzu TGA-50 apparatus from 30 to 800 °C with a temperature-programmed rate of 10 °C min^{-1} in an oxygen atmosphere.

2.5. Catalytic tests

The MTO reaction was carried out at 425 °C under atmospheric pressure in a fixed bed reactor of a quartz tube with an internal diameter of 10 mm and a total length of 370 mm. In a typical run, 1 g of the ZnSAPO-34 catalyst (20–40 mesh) was diluted with 1 g of quartz sand particles (20–40 mesh) before being introduced into the middle section of the reactor. The catalyst was first activated at 425 °C for 1 h under N_2 at a flow rate of 60 mL min^{-1}. After the activation, the flow rate of N_2 was constantly maintained at 60 mL min^{-1} as carrier gas. A liquid solution of methanol and H_2O (50 mol %) was fed by an high-pressure liquid chromatography (HPLC) pump into the reactor, and the weight hourly space velocity of the methanol was 2 h^{-1}. The reaction products were analyzed using an online gas chromatograph (SP-2100) equipped with a flame ionization detector and a KB-PLOT-QP capillary column (50 m × 0.32 mm × 10 μm). The initial temperature of the column was set at 60 °C for 4 min, then the temperature was increased to 180 °C with a ramping rate of 20 °C min^{-1} and held at 180 °C for 10 min. The effluent line of the reaction system was heated in case of condensation of heavy hydrocarbons. The conversion of methanol and selectivity of products were calculated on CH_2 basis. Dimethyl ether was considered to be unreacted species instead of a product in the calculation.

3. Results and discussion

3.1. Catalyst characterization

The X-ray power diffraction patterns of SAPO-34, ZnSAPO-34, and ZnSAPO-34-*x* are shown in Fig. 1 and the relative crystallinities are given in Table 1. SAPO-34 and ZnSAPO-34 exhibit the similar characteristic diffraction peaks, corresponding to the chabazite-type structure [3]. In addition, broadening of diffraction peaks for ZnSAPO-34 is observed due to the smaller size of ZnSAPO-34 with the incorporation of Zn. No diffraction peaks belonged to Zn-related species are observed on ZnSAPO-34, presumably owing to the uniform dispersion of Zn species in the zeolites and the low level of Zn-loading in the synthesis [36]. It is worth noting that the peaks of ZnSAPO-34 slightly shift toward lower angles compared with SAPO-34, which can be ascribed to an increase in the interplanar spacing in ZnSAPO-34. This phenomenon confirms the successful incorporation of Zn^{2+} into the SAPO-34 framework, in accordance with the results reported for MeSAPO-34 samples [37–39]. Notably, after the TEAOH treatment, no extra peaks are discerned, suggesting that the framework of ZnSAPO-34 is well preserved. However, as shown in Table 1, with the increase in the concentrations of TEAOH, the relative crystallinities gradually decrease. The gradual loss of crystallinity may stem from the defects generated by alkali treatment [36].

Fig. 2 presents the SEM images of SAPO-34, ZnSAPO-34, and ZnSAPO-34-*x* samples. SAPO-34 (Fig. 2a) represents the typical cubic morphology with particle sizes of about 3–5 μm. In comparison, the crystal size of ZnSAPO-34 (Fig. 2b) is much smaller than that of SAPO-34. Thus, the introduction of Zn species reduces the crystal size of SAPO-34, indicating that the presence of Zn species in the initial gel may increase the nucleation rate [37,40]. It is noteworthy that all the treated ZnSAPO-34 crystals exhibit rough surface owing to the etching with the TEAOH solution. Specifically, when the concentration of TEAOH is less than 0.3 mol L^{-1}, the surface is slightly etched by TEAOH and the grooves on the surface are clearly visible. When

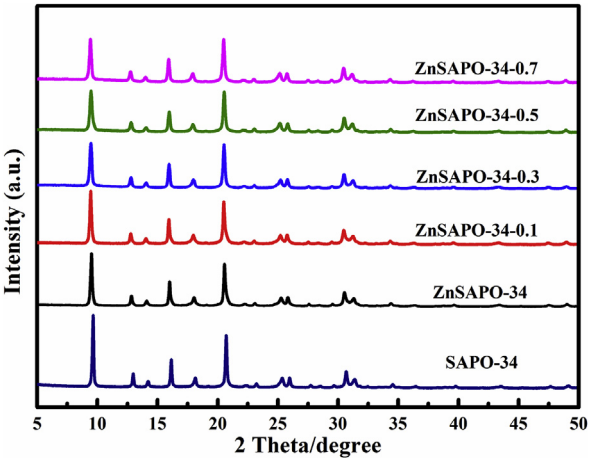

Fig. 1. XRD patterns of SAPO-34, ZnSAPO-34, and ZnSAPO-34-*x*.

Table 1
Textural properties of the as-prepared samples.

Samples	Chemical composition[a] (mol)	Relative crystallinity[b]
SAPO-34	$Al_{0.470}P_{0.351}Si_{0.178}O_2$	109.5
ZnSAPO-34	$Al_{0.448}P_{0.339}Si_{0.198}Zn_{0.015}O_2$	100
ZnSAPO-34-0.1	$Al_{0.455}P_{0.342}Si_{0.185}Zn_{0.018}O_2$	95.9
ZnSAPO-34-0.3	$Al_{0.456}P_{0.343}Si_{0.169}Zn_{0.023}O_2$	91.0
ZnSAPO-34-0.5	$Al_{0.469}P_{0.350}Si_{0.155}Zn_{0.026}O_2$	85.1
ZnSAPO-34-0.7	$Al_{0.476}P_{0.361}Si_{0.133}Zn_{0.030}O_2$	75.9

[a] Measured by ICP-OES.
[b] The crystallinity of ZnSAPO-34 is defined as 100%.

treated with a more concentrated solution (0.5 mol L^{-1}), the sample (Fig. 2e) shows that the large macropores are formed in ZnSAPO-34-0.5. Moreover, as can be seen from Fig. 2f, further increase in the TEAOH concentrations (0.7 mol L^{-1}) leads to more deeply etched crystals and large voids are created in ZnSAPO-34.

TEM images of ZnSAPO-34, ZnSAPO-34-0.5, and ZnSAPO-34-0.7 are shown in Fig. 3 to further depict the detailed features of the zeolites. TEM image of the parent ZnSAPO-34 (Fig. 3a) presents no obvious black particles, demonstrating that no aggregation of ZnO particles exists. As illustrated in Fig. 3b, when the concentration of TEAOH is 0.5 mol L^{-1}, large macropores penetrated through the entire crystals are

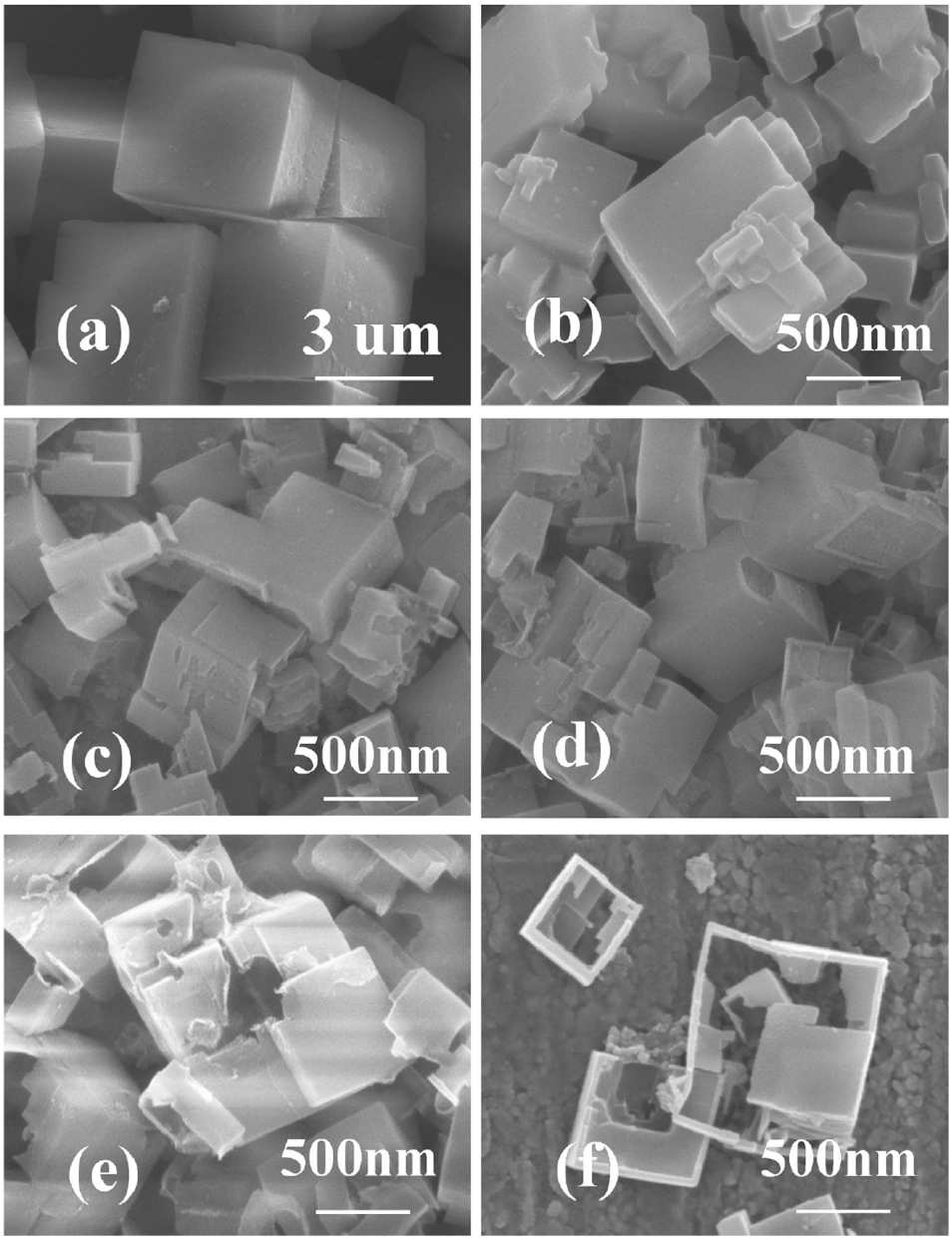

Fig. 2. SEM images of SAPO-34 (a), ZnSAPO-34 (b), ZnSAPO-34-0.1 (c), ZnSAPO-34-0.3 (d), ZnSAPO-34-0.5 (e), and ZnSAPO-34-0.7 (f).

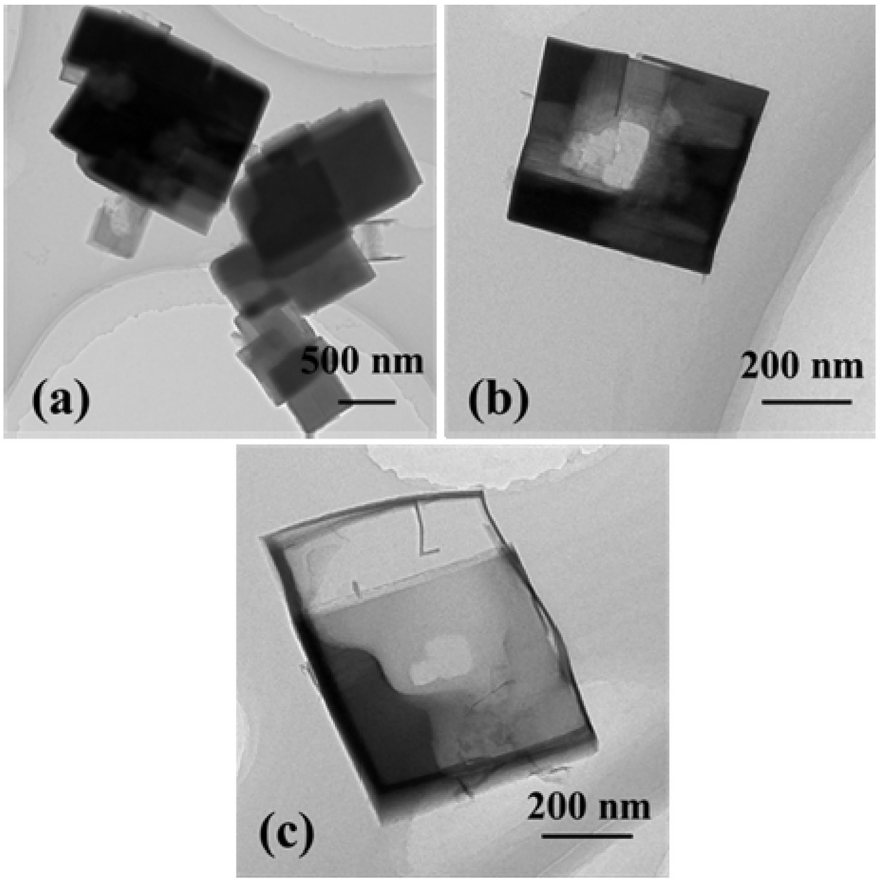

Fig. 3. TEM images of SAPO-34 (a), ZnSAPO-34-0.5 (b), and ZnSAPO-34-0.7 (c).

constructed in ZnSAPO-34-0.5. With further increase in the TEAOH concentration to 0.7 mol L^{-1}, the center-hollowed morphology with large voids is created in the ZnSAPO-34-0.7 crystals, as shown in Fig. 3c. Zhang et al. [24] reported that the growth of SAPO-34 followed the surface to core crystal growth route. It means that the core of the crystals is relatively less crystallized than the shell and easily attacked by the alkaline TEAOH. This might be the reason for the formation of the center-hollowed morphology after TEAOH treatment. The center-hollowed morphology with big holes at the central parts of the crystals was also observed in hydrofluoric acid (HF) etching of SAPO-34 [41].

The compositions of the as-synthesized samples determined by ICP-OES are given in Table 1. As shown in Table 1, the introduction of Zn results in a slight decrease in the Si content compared with the parent SAPO-34. The decrease in Si contents means that the introduction of Zn may affect the Si substitution into the frameworks of SAPO-34. This result agrees well with the findings of Liu et al. [38] that the presence of Mg has an influence on the Si substitution into the framework of SAPO-34. Furthermore, after the post-treatment of TEAOH, Al, P, and Zn contents of the ZnSAPO-34-*x* gradually increase with increase in the TEAOH concentration, whereas the Si contents gradually decrease. This observation proves that the TEAOH preferentially extracts the Si species of ZnSAPO-34.

The N_2 adsorption/desorption isotherms of SAPO-34, ZnSAPO-34, and ZnSAPO-34-*x* are presented in Fig. 4 and the textural properties of the samples are listed in Table 2. Obviously, the parent SAPO-34 shows a typical type I isotherm, characteristic of microporosity. ZnSAPO-34 sample also displays the characteristics of the type I

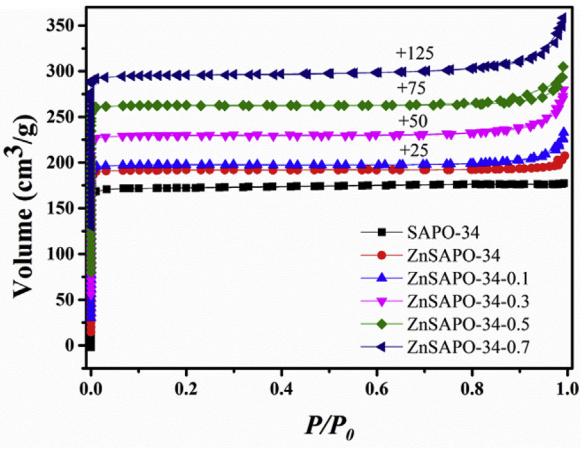

Fig. 4. N_2 adsorption/desorption isotherms of SAPO-34, ZnSAPO-34, and ZnSAPO-34-*x*.

Table 2
Textural properties of SAPO-34, ZnSAPO-34, and ZnSAPO-34-*x*.

Samples	Surface area ($m^2\ g^{-1}$)			Pore volume ($cm^3\ g^{-1}$)		
	S_{BET} [a]	S_{micro} [b]	S_{ext} [b]	V_{total} [c]	V_{micro} [d]	V_{sec} [e]
SAPO-34	617	606	11	0.291	0.281	0.010
ZnSAPO-34	720	685	35	0.349	0.327	0.022
ZnSAPO-34-0.1	696	654	42	0.338	0.312	0.026
ZnSAPO-34-0.3	680	631	49	0.327	0.298	0.029
ZnSAPO-34-0.5	663	608	55	0.315	0.278	0.037
ZnSAPO-34-0.7	625	540	85	0.283	0.204	0.079

[a] S_{BET} (total surface area) was calculated from the BET model.
[b] S_{micro} (micropore surface area) was determined by the *t*-plot method, $S_{ext} = S_{BET} - S_{micro}$.
[c] Evaluated at $p/p_0 = 0.99$.
[d] V_{micro} (micropore volume) was evaluated by the *t*-plot method.
[e] V_{sec} (secondary macropore volume) $= V_{total} - V_{micro}$.

isotherm, although a slightly enhanced uptake of the isotherms near saturation pressure ($P/P_0 > 0.9$) is discerned due to the intercrystal porosity of small particles. The latter observation verifies the small size of ZnSAPO-34 crystallites [13,31,42], which is also evidenced by the SEM results (Fig. 2b). With the incorporation of Zn into SAPO-34, the resulting ZnSAPO-34 exhibits a substantial increase in the total surface areas (from 617 to 720 $m^2\ g^{-1}$) and total volumes (from 0.291 to 0.349 $cm^3\ g^{-1}$) due to the considerable reduction in crystal size. After the TEAOH treatment, all samples still display the characteristic type I isotherms. Furthermore, a more pronounced ascent of the isotherms at higher relative pressure ($P/P_0 > 0.9$) is discerned, which is associated with nitrogen adsorption in macropores [41,43,44], agreeing with SEM and TEM results in which large pores are clearly visible. As listed in Table 2, after the TEAOH treatment, there is a slight reduction in the total surface areas and the microporous surface areas when the concentration of TEAOH is less than 0.5 mol L^{-1}, which reflects a good preservation of microporosity of the ZnSAPO-34 crystals after the TEAOH post-treatment. The external surface areas of the obtained hierarchical ZnSAPO-34-*x* do not change appreciably under the above treatment conditions. However, with further increase in the severity of TEAOH treatment (0.7 mol L^{-1}), the total surface area of ZnSAPO-34-0.7 decreases considerably. On the contrary, the external surface area and secondary macropore volume of ZnSAPO-34-0.7 increase significantly, with dramatic decrease in the microporous surface area and microporous volume.

The FTIR spectra of SAPO-34, ZnSAPO-34, and ZnSAPO-34-*x* are presented in Fig. 5. For SAPO-34, the framework vibrations are characteristically in agreement with those of the relevant reports [5,45–48]. The absorption peaks at 490 and 632 cm^{-1} are assigned to T–O bending bands of TO_4 tetrahedral and D-6 rings, respectively. Peaks at 725 and 1100 cm^{-1} correspond to asymmetric and symmetric vibrations of O–P–O, respectively. The peak at the wavenumber of 1651 cm^{-1} can be attributed to the vibration of hydroxyl groups from physically adsorbed water. Furthermore, the band at 3445 cm^{-1} can be attributed to the stretching vibration of the bridging hydroxyl groups, that is, Si–OH–Al, which plays an important role in the MTO reaction [8]. As to ZnSAPO-34, the

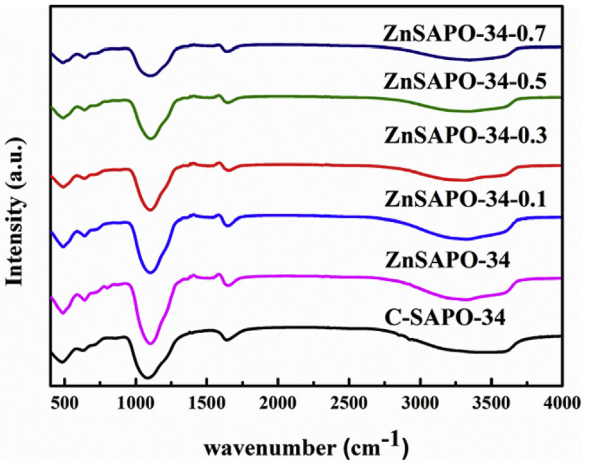

Fig. 5. FTIR profiles of SAPO-34, ZnSAPO-34, and ZnSAPO-34-*x*.

characteristic peak positions are similar to those of SAPO-34. However, the incorporation of Zn results in the shift of the peak positions and the change in the intensity of the structure-sensitive bands. For example, the band at 632 cm^{-1} is shifted to around 640 cm^{-1}. It is important to highlight that the shift in the absorption bands is considered as evidence for metal ions incorporating into the framework of SAPO-34 [35]. Moreover, the major peaks of ZnSAPO-34 are retained after the TEAOH treatment, suggesting that the framework of ZnSAPO-34 is well preserved. These results are in good agreement with the corresponding XRD analysis.

NH_3-TPD profiles of the samples are shown in Fig. 6, and their acid amounts are presented in Table 3. There are two distinct peaks in NH_3-TPD for all samples at 200–350 and 400–500 °C, which are assigned to the weak and strong acid sites, respectively. The low temperature peak is attributed to the external surface hydroxyl groups such as T–OH (T = Si, P, Al), whereas the high temperature peak corresponds to the structure acidity [42,46]. It is believed that the weak acid sites are not responsible for the MTO

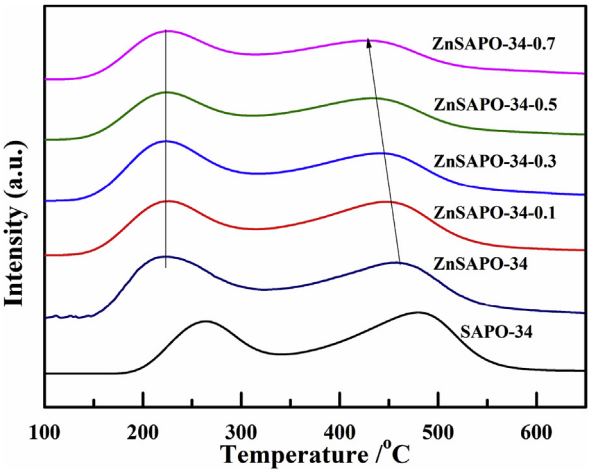

Fig. 6. NH_3-TPD profiles of SAPO-34, ZnSAPO-34, and ZnSAPO-34-*x*.

Table 3
Acid amounts of samples.

Samples	Acid amounts[a] (mmol g^{-1})		
	Total acidity	Strong acidity	Weak acidity
SAPO-34	1.129	0.584	0.545
ZnSAPO-34	1.098	0.548	0.550
ZnSAPO-34-0.1	1.059	0.528	0.531
ZnSAPO-34-0.3	1.035	0.524	0.511
ZnSAPO-34-0.5	0.988	0.503	0.485
ZnSAPO-34-0.7	0.914	0.479	0.435

[a] Calculated by NH_3-TPD.

reactions [27,49]. Consequently, we are mainly concerned with the changes in the strong acid sites. As it can be seen, compared with the parent SAPO-34, the desorption peak of ZnSAPO-34 at the high temperature shifts toward lower temperature with the incorporation of Zn. This shift suggests the decrease in acid strength in the strong acid sites of ZnSAPO-34. Moreover, the peak area of ZnSAPO-34 at the high temperature decreases compared to the parent SAPO-34, which means lower acid concentration in the strong acid sites of ZnSAPO-34. It should be pointed out that a lower Si/Al ratio results in the milder acidity [50]. As a result, the decreased acid strength and lower acid concentration in the strong acid sites of ZnSAPO-34 stem from less Si incorporation owing to the isomorphous substitution of Zn and this is consistent with the ICP results [35,38].

With increase in the severity of the TEAOH treatment, the positions of the peaks at the high temperatures of the hierarchical ZnSAPO-34 gradually shift to lower temperatures. The peak areas of the hierarchical ZnSAPO-34-*x* at high temperature gradually decrease with increase in the concentration of TEAOH. The results reveal that the acid strength and the acid concentrations in the strong acid sites of the resulting hierarchical ZnSAPO-34-*x* are lower than those of the parent ZnSAPO-34. The results show good agreement between the decreased Si contents and the relatively weak acidity of the post-treated ZnSAPO-34-*x* samples.

3.2. Catalytic performance in the MTO reaction

The catalytic properties of SAPO-34, ZnSAPO-34, and ZnSAPO-34-*x* were evaluated in the MTO reaction. The methanol conversion, selectivity of ethylene plus propylene ($C_2^=-C_3^=$), selectivity of propylene, and selectivity of ethylene as a function of reaction time on stream (TOS) are illustrated in Fig. 7. In this work, the catalyst lifetime here represents for the reaction duration from the beginning to the time when the methanol conversion drops below 99%. As shown in Fig. 7a and b, compared with the parent SAPO-34, both the lifetime and the $C_2^=-C_3^=$ selectivity of ZnSAPO-34 are greatly improved after the introduction of Zn. Such an improvement of the catalytic performance can be attributed to the reduction in the crystal size, the decreased acid strength, and the decreased acid concentration of the strong acid sites of the zeolite [14,51,52].

As illustrated in Fig. 7b, the $C_2^=-C_3^=$ selectivities of the hierarchical ZnSAPO-34-*x* are further increased with the

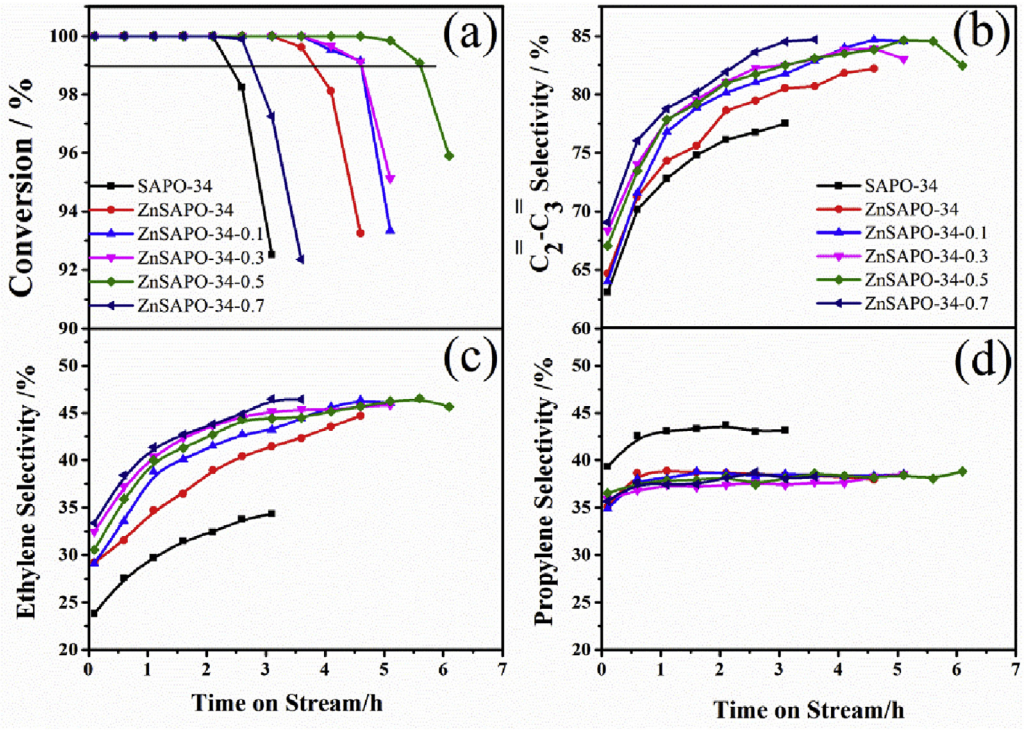

Fig. 7. Methanol conversion (a), propylene plus ethylene selectivity (b), selectivity of propylene (c), and selectivity of ethylene (d) of the MTO reaction with TOS over SAPO-34, ZnSAPO-34, and ZnSAPO-34-*x* catalysts.

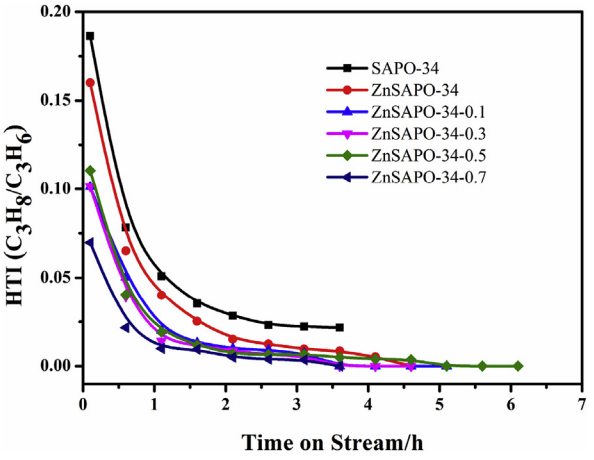

Fig. 8. HTI (C_3H_8/C_3H_6) values of methanol conversion over SAPO-34, ZnSAPO-34, and ZnSAPO-34-*x*.

post-treatment of TEAOH, nearly 4% higher than that of the parent ZnSAPO-34 catalyst. The lifetime of the hierarchical ZnSAPO-34-*x* varies with different TEAOH concentrations for the post-treatment. When the concentration of TEAOH is less than 0.5 mol L^{-1}, the hierarchical ZnSAPO-34-*x* exhibits longer catalytic lifetime than the parent ZnSAPO-34 catalyst. Particularly, when the TEAOH concentration is 0.5 mol L^{-1}, the obtained hierarchical ZnSAPO-34-0.5 shows the longest catalytic lifetime, approximately 2 h longer than the parent ZnSAPO-34. The prominent enhancement of the catalytic performance of the hierarchical ZnSAPO-34-*x* in the MTO reaction is associated with the enhanced diffusion efficiency, decreased acid strength, and low acid concentrations of the strong acid sites. On one hand, the generated macropores in the hierarchical ZnSAPO-34 can greatly facilitate the mass transfer of the reactant and products, thus prolong the catalytic lifetime of the catalysts [12,26,31]. On the other hand, the decreased acid strength and acid concentrations in the strong acid sites of the hierarchical ZnSAPO-34-*x* catalysts can also improve the catalytic lifetime and the $C_2^=-C_3^=$ selectivity of the catalysts [26]. However, with more severe TEAOH treatment condition (0.7 mol L^{-1}), the catalytic lifetime of ZnSAPO-34-0.7 drastically decreases. According to the literature, SAPO-34 with mild acidity is more appropriate to catalyze the MTO reaction [11,53]. However, too less acid sites would be detrimental for the catalytic lifetime of SAPO-34 [54,55]. Accordingly, the significantly reduced crystallinity and too less strong acid sites are supposed to be responsible for the short catalytic lifetime of ZnSAPO-34-0.7 [42].

As it can be seen from Fig. 7c and d, compared with the parent SAPO-34, ZnSAPO-34 exhibits higher selectivity of ethylene but lower selectivity of propylene. Moreover, after the TEAOH treatment, the selectivity of ethylene over hierarchical ZnSAPO-34-*x* is obviously higher than that of the parent ZnSAPO-34, whereas the selectivity of propylene over the hierarchical ZnSAPO-34-*x* is comparable to that of the parent ZnSAPO-34. It is proposed that the decreased acidity could improve the selectivity of ethylene in the MTO reaction [56]. Consequently, the improvement in the selectivity of ethylene can be attributed to the decreased acid strength and the decreased amounts of the strong acid of the hierarchical ZnSAPO-34-*x* zeolites.

Fig. 8 depicts the hydrogen transfer index (HTI, C_3H_8/C_3H_6 ratio) values of methanol conversion over SAPO-34, ZnSAPO-34, and ZnSAPO-34-*x*. The $C_2^=-C_3^=$ selectivity and the catalytic life are closely related to the side reactions, such as hydrogen transfer reaction, oligomerization, isomerization, and aromatization [38,51]. In this work, the HTI value is used to evaluate the hydrogen transfer level of SAPO-34, ZnSAPO-34, and ZnSAPO-34-*x* catalysts. As shown in Fig. 8, all the catalysts have high HTI values during the initial reaction stage, which means higher propane selectivity. Then the HTI values gradually decrease with TOS. HTI value of ZnSAPO-34 is lower than that of SAPO-34

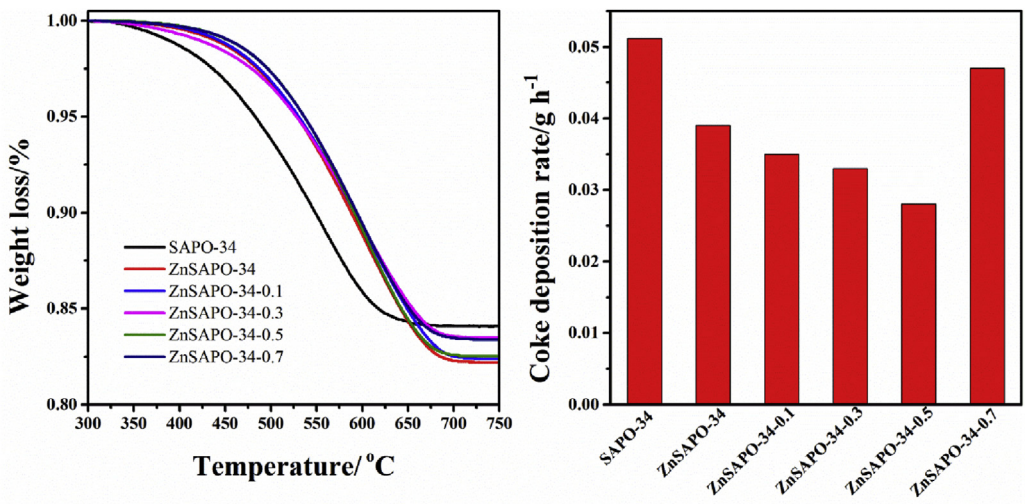

Fig. 9. TGA profiles and carbon deposition rates of deactivated SAPO-34, ZnSAPO-34, and ZnSAPO-34-*x* in MTO reactions.

due to the decreased acidity and the small crystal size with the incorporation of Zn. The HTI values of the hierarchical ZnSAPO-34-*x* are much lower than that of the parent ZnSAPO-34. When the concentration of TEAOH is less than 0.5 mol L^{-1}, lower HTI values over the hierarchical ZnSAPO-34-*x* correspond to higher $C_2^=-C_3^=$ selectivity and longer catalytic lifetime, which can be attributed to the increased mass transfer of coke precursors, decreased acid strength, and decreased acid concentrations of the strong acid sites of the hierarchical ZnSAPO-34-*x* after the post-treatment of TEAOH [13]. Notably, ZnSAPO-34-0.7 has the lowest HTI value and the highest $C_2^=-C_3^=$ selectivity. However, ZnSAPO-34-0.7 has shorter catalytic lifetime than the parent ZnSAPO-34 because of the significantly reduced crystallinity and too less strong acid sites.

After the reaction, the coke formation of the deactivated zeolites was further measured by thermal analysis. Fig. 9 shows the results of the weight loss and the coke deposition rate of the deactivated zeolites. The weight losses of the catalysts over the temperature range of 300–750 °C are owing to combustion of the deposited coke species. The coke deposition rates are obtained by dividing the amounts of the deposited coke species with the reaction TOS. The amount of the coke content over ZnSAPO-34 is higher than that of SAPO-34; however, the coke deposition rate of ZnSAPO-34 is much lower than that of SAPO-34 because of the longer catalytic lifetime of ZnSAPO-34. The coke deposition rates of ZnSAPO-34-*x* are lower than that of the parent ZnSAPO-34 when the concentration of TEAOH is less than 0.5 mol L^{-1}. The lower coke deposition rate of ZnSAPO-34-*x* is consistent with the lower HTI (Fig. 8) and the longer catalytic lifetime of ZnSAPO-34-*x* when the concentration of TEAOH is less than 0.5 mol L^{-1}. However, the coke deposition rate of ZnSAPO-34-0.7 is higher than that of the parent ZnSAPO-34, owing to the shorter lifetime.

4. Conclusions

Hierarchical ZnSAPO-34 zeolites can be prepared with the post-treatment of TEAOH. After the post-treatment of TEAOH, macropores are created in the central parts of the ZnSAPO-34 zeolite at relatively higher TEAOH concentrations. The formation of hierarchical ZnSAPO-34 could intensify the mass transport of the reactants and products in the MTO reaction. Moreover, the alkaline treatment could modulate the acidity of ZnSAPO-34 through preferential dissolution of Si contents. In the MTO reaction, the hierarchical ZnSAPO-34 zeolites exhibit prolonged catalytic lifetime and considerable enhancement of the $C_2^=-C_3^=$ selectivity, which can be attributed to the mild acidity and the improved mass transfer of the hierarchical ZnSAPO-34 zeolite.

Acknowledgments

This work has been supported by the National Natural Science Foundation of China (grant no. 21276183).

References

[1] J. Ahmadpour, M. Taghizadeh, C. R. Chimie 18 (2015) 834.
[2] P. Losch, M. Boltz, B. Louis, S. Chavan, U. Olsbye, C. R. Chimie 18 (2015) 330.
[3] J. Tan, Z.M. Liu, X.H. Bao, X.C. Liu, X.W. Han, C.Q. He, R.S. Zhai, Microporous Mesoporous Mater. 53 (2002) 97.
[4] D.R. Dubois, D.L. Obrzut, J. Liu, J. Thundimadathil, P.M. Adekkanattu, J.A. Guin, A. Punnoose, M.S. Seehra, Fuel Process. Technol. 83 (2003) 203.
[5] M. Salmasi, S. Fatemi, A. Taheri Najafabadi, J. Ind. Eng. Chem. 17 (2011) 755.
[6] F.C. Sena, B.F. de Souza, N.C. de Almeida, J.S. Cardoso, L.D. Fernandes, Appl. Catal. A 406 (2011) 59.
[7] T. Álvaro-Muñoz, C. Márquez-Álvarez, E. Sastre, Catal. Today 179 (2012) 27.
[8] S. Aghamohammadi, M. Haghighi, M. Charghand, Mater. Res. Bull. 50 (2014) 462.
[9] D. Fan, P. Tian, S.T. Xu, D.H. Wang, Y. Yang, J.Z. Li, Q.Y. Wang, M. Yang, Z.M. Liu, New J. Chem. 40 (2016) 4236.
[10] P.F. Wang, A. Lv, J. Hu, J.A. Xu, G.Z. Lu, Microporous Mesoporous Mater. 152 (2012) 178.
[11] U. Olsbye, S. Svelle, M. Bjorgen, P. Beato, T.V. Janssens, F. Joensen, S. Bordiga, K.P. Lillerud, Angew. Chem. Int. Ed. 51 (2012) 5810.
[12] X.X. Chen, A. Vicente, Z.X. Qin, V. Ruaux, J.P. Gilson, V. Valtchev, Chem. Commun. 52 (2016) 3512.
[13] M. Yang, P. Tian, C. Wang, Y.Y. Yuan, Y. Yang, S.T. Xu, Y.L. He, Z.M. Liu, Chem. Commun. 50 (2014) 1845.
[14] C. Wang, M. Yang, M.R. Li, S.T. Xu, Y. Yang, P. Tian, Z.M. Liu, Chem. Commun. 52 (2016) 6463.
[15] L. Tosheva, V.P. Valtchev, Chem. Mater. 17 (2005) 2494.
[16] V. Valtchev, L. Tosheva, Chem. Rev. 113 (2013) 6734.
[17] S. Mintova, M. Jaber, V. Valtchev, Chem. Soc. Rev. 44 (2015) 7207.
[18] L.H. Chen, X.Y. Li, J.C. Rooke, Y.H. Zhang, X.Y. Yang, Y. Tang, F.S. Xiao, B.L. Su, J. Mater. Chem. 22 (2012) 17381.
[19] Y. Wei, T.E. Parmentier, K.P. de Jong, J. Zecevic, Chem. Soc. Rev. 44 (2015) 7234.
[20] Y. Hirota, K. Murata, S. Tanaka, N. Nishiyama, Y. Egashira, K. Ueyama, Mater. Chem. Phys. 123 (2010) 507.
[21] S. Lin, J.Y. Li, R.P. Sharma, J.H. Yu, R.R. Xu, Top. Catal. 53 (2010) 1304.
[22] S. Askari, R. Halladj, Ultrason. Sonochem. 19 (2012) 554.
[23] F. Schmidt, S. Paasch, E. Brunner, S. Kaskel, Microporous Mesoporous Mater. 164 (2012) 214.
[24] J. Gong, F. Tong, X.B. Ji, C.F. Zeng, C.Q. Wang, Y. Lv, L.X. Zhang, Cryst. Growth Des. 14 (2014) 3857.
[25] Q.M. Sun, N. Wang, D.Y. Xi, M. Yang, J.H. Yu, Chem. Commun. 50 (2014) 6502.
[26] Q.M. Sun, N. Wang, G.Q. Guo, X.X. Chen, J.H. Yu, J. Mater. Chem. A 3 (2015) 19783.
[27] A.Z. Varzaneh, J. Towfighi, S. Sahebdelfar, H. Bahrami, J. Anal. Appl. Pyrolysis 121 (2016) 11.
[28] J.C. Groen, L.A. Peffer, J.A. Moulijn, J. Pérez-Ramírez, Chem. Eur. J. 11 (2005) 4983.
[29] V. Valtchev, G. Majano, S. Mintova, J. Pérez-Ramírez, Chem. Soc. Rev. 42 (2013) 263.
[30] X. Liu, S. Ren, G.F. Zeng, G.J. Liu, P. Wu, G. Wang, X.Q. Chen, Z.Y. Liu, Y.H. Sun, RSC Adv. 6 (2016) 28787.
[31] X.X. Chen, D.Y. Xi, Q.M. Sun, N. Wang, Z.Y. Dai, D. Fan, V. Valtchev, J.H. Yu, Microporous Mesoporous Mater. 234 (2016) 401.
[32] Y.Y. Qiao, M. Yang, B.B. Gao, L.Y. Wang, P. Tian, S.T. Xu, Z.H. Liu, Chem. Commun. 52 (2016) 5718.
[33] Y.X. Wei, Y.L. He, D.Z. Zhang, L. Xu, S.H. Meng, Z.M. Liu, B.L. Su, Microporous Mesoporous Mater. 90 (2006) 188.
[34] M. Hartmann, L. Kevan, Chem. Rev. 99 (1999) 635.
[35] L. Xu, Z.M. Liu, A.P. Du, Y.X. Wei, Z.G. Sun, Stud. Surf. Sci. Catal. 147 (2004) 445.
[36] C.G. Yang, M.H. Qiu, S.W. Hu, X.Q. Chen, G.F. Zeng, Z.Y. Liu, Y.H. Sun, Microporous Mesoporous Mater. 231 (2016) 110.
[37] Y.Y. Zhang, L. Chen, Y.F. Li, Y.Q. Deng, C.T. Au, S.F. Yin, React. Kinet. Mech. Catal. 115 (2015) 691.
[38] D.Z. Zhang, Y.X. Wei, L. Xu, F.X. Chang, Z.Y. Liu, S.H. Meng, B.L. Su, Z.M. Liu, Microporous Mesoporous Mater. 116 (2008) 684.
[39] F. Marzpour Shalmani, R. Halladj, S. Askari, RSC Adv. 7 (2017) 26756.
[40] A.Z. Varzaneh, J. Towfighi, S. Sahebdelfar, Microporous Mesoporous Mater. 236 (2016) 1.
[41] D.Y. Xi, Q.M. Sun, J. Xu, M. Cho, H.S. Cho, S. Asahina, Y. Li, F. Deng, O. Terasaki, J.H. Yu, J. Mater. Chem. A 2 (2014) 17994.
[42] Q.M. Sun, Y.H. Ma, N. Wang, X. Li, D.Y. Xi, J. Xu, F. Deng, K.B. Yoon, P. Oleynikov, O. Terasaki, J.H. Yu, J. Mater. Chem. A 2 (2014) 17828.
[43] Z. Qin, L. Lakiss, J.P. Gilson, K. Thomas, J.M. Goupil, C. Fernandez, V. Valtchev, Chem. Mater. 25 (2013) 2759.

[44] C.Y. Dai, A.F. Zhang, L.L. Li, K.K. Hou, F.S. Ding, J. Li, D.Y. Mu, C.S. Song, M. Liu, X.W. Guo, Chem. Mater. 25 (2013) 4197.
[45] M. Charghand, M. Haghighi, S. Aghamohammadi, Ultrason. Sonochem. 21 (2014) 1827.
[46] J.Q. Li, Z. Li, D.Z. Han, J.H. Wu, Powder Technol. 262 (2014) 177.
[47] S. Aghamohammadi, M. Haghighi, Chem. Eng. J. 264 (2015) 359.
[48] E. Aghaei, M. Haghighi, J. Porous Mater. 22 (2015) 187.
[49] L.P. Ye, F.H. Cao, W.Y. Ying, D.Y. Fang, Q.W. Sun, J. Porous Mater. 18 (2011) 225.
[50] Y.X. Li, Y.H. Huang, J.H. Guo, M.Y. Zhang, D.Z. Wang, F. Wei, Y. Wang, Catal. Today 233 (2014) 2.
[51] G.J. Yang, Y.X. Wei, S.T. Xu, J.R. Chen, J.Z. Li, Z.M. Liu, J.H. Yu, R.R. Xu, J. Phys. Chem. C 117 (2013) 8214.
[52] G.Y. Liu, P. Tian, J.Z. Li, D.Z. Zhang, F. Zhou, Z.M. Liu, Microporous Mesoporous Mater. 111 (2008) 143.
[53] L.T. Yuen, S.I. Zones, T.V. Harris, E.J. Gallegos, A. Auroux, Microporous Mater. 2 (1994) 105.
[54] S. Wilson, P. Barger, Microporous Mesoporous Mater. 29 (1999) 117.
[55] C. Wang, M. Yang, P. Tian, S.T. Xu, Y. Yang, D.H. Wang, Y.Y. Yuan, Z.M. Liu, J. Mater. Chem. A 3 (2015) 5608.
[56] M. Kang, T. Inui, Catal. Lett. 53 (1998) 171.